Analysis of Changes in Gene Expression and Metabolic Profiles Induced by Silica-Coated Magnetic Nanoparticles

Wooyoung Shim,[†,▽] Man Jeong Paik,[‡,▽] Duc-Toan Nguyen,[†] Jin-Kyu Lee,[§] Yuwon Lee,[§] Jae-Ho Kim,[†] Eun-Hee Shin,[⊥,∥] Jin Seok Kang,[¶] Hak-Sung Jung,[§] Sangdun Choi,[†] Sungsu Park,[#,▲] Jeom Soon Shim,[†] and Gwang Lee[†,△,*]

[†]Department of Molecular Science and Technology, Ajou University, Suwon, Republic of Korea, [‡]College of Pharmacy, Sunchon National University, Suncheon, Republic of Korea, [§]Department of Chemistry, Seoul National University, Republic of Korea, [⊥]Department of Parasitology and Tropical Medicine, Seoul National University College of Medicine, Seoul, Republic of Korea, [∥]Seoul National University Bundang Hospital, Seongnam, Republic of Korea, [¶]Department of Biomedical Laboratory Science, Namseoul University, Cheonan, Republic of Korea, [#]Department of Chemistry and Nano Science, Ewha Womans University, Seoul, Republic of Korea, [▲]Mechanobiology Institute, National University of Singapore, Singapore, and [△]Institute for Medical Sciences, Ajou University School of Medicine, Suwon, Republic of Korea. [▽]These authors contributed equally to this work.

ABSTRACT Magnetic nanoparticles (MNPs) have proven themselves to be useful in biomedical research; however, previous reports were insufficient to address the potential dangers of nanoparticles. Here, we investigated gene expression and metabolic changes based on the microarray and gas chromatography—mass spectrometry with human embryo kidney 293 cells treated with MNPs@SiO_2(RITC), a silica-coated MNP containing Rhodamine B isothiocyanate (RITC). In addition, measurement of reactive oxygen species (ROS) and ATP analysis were performed to evaluate the effect of MNPs@SiO_2(RITC) on mitochondrial function. Compared to the nontreated control, glutamic acid was increased by more than 2.0-fold, and expression of genes related to the glutamic acid metabolic pathway was also disturbed in 1.0 μg/μL of MNPs@SiO_2(RITC)-treated cells. Furthermore, increases in ROS concentration and mitochondrial damage were observed in this MNPs@SiO_2(RITC) concentration. The organic acids related to the Krebs cycle were also disturbed, and the capacity of ATP synthesis was decreased in cell treated with an overdose of MNPs@SiO_2(RITC). Collectively, these results suggest that overdose (1.0 μg/μL) of MNPs caused transcriptomic and metabolic disturbance. In addition, we suggest that a combination of gene expression and metabolic profiles will provide more detailed and sensitive toxicological evaluation for nanoparticles.

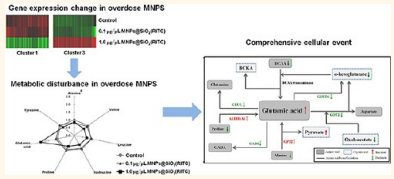

KEYWORDS: magnetic nanoparticles · cytotoxicity · microarray · metabolism · mitochondria

Development of nanotechnology has resulted in a reduction of particle sizes, which improves cellular uptake efficiencies and endows novel physical properties that are potentially useful in biomedical research.[1,2] Magnetic nanoparticles (MNPs), which are defined as single-dimensional particles with magnetic properties and of average size less than 100 nm, have recently been examined in the context of novel applications as drug nanocarrier, magnetic resonance (MR) imaging contrast agents, gene delivery, and antibody engineering.[3−7] Scarberry *et al.* reported successful targeting of cancer cells *in vitro* and *in vivo* using MNPs conjugated to peptides and demonstrated that MNPs can be used as biosensors and diagnostic tools for cancer.[8] Although MNPs have a strong potential for practical application in nanomedicine, studies of the biological effects of MNPs are demanded as essential factors. However, only a few studies have been performed on the toxicity of MNPs using the 3-(4,5-dimethylthiazol-2-yl)-2,5-diphenyltetrazolium bromide (MTT) assay, chromosome aberration assay, hematoxylin and eosin (H&E) staining, and *in vivo* tissue distribution.[9−12] Information obtained from previous reports has been restricted to pathological effects of MNPs.

To obtain comprehensive information for the phenomenon related with the biological mechanism which was influenced by MNPs, investigation of cellular metabolite is highly necessary. The cellular metabolites including amino acids (AAs) and organic acids (OAs) are well-known as important components of cells, nutrients, biocatalysts, and neurotransmitters.[13−18] For instance, glutamic acid, known as one of the proteinogenic and nonessential AAs, plays an important role in neurological processes such as precursor of neural molecules. Glutamic acid is transaminated to γ-aminobutyric acid (GABA) and glutamine by

* Address correspondence to glee@ajou.ac.kr.

Received for review March 14, 2012 and accepted July 24, 2012.

Published online July 24, 2012
10.1021/nn301113f

glutamate decarboxylase (GAD) and glutamate ammonia ligase (GLUL), respectively.[19−21] In addition, glutamic acid is converted into pyruvate, α-ketoglutarate, and oxaloacetate, which are major molecules for generation of cellular energy, and pyruvate is also decarboxylated to synthesize acetyl-CoA by pyruvate dehydrogenase complex (PDC) in the Krebs cycle.[22−24] Although metabolite profiling analysis is important for explanation of comprehensive cellular events, it was not sufficiently studied that metabolites could be influenced by nanomaterials.

MNPs@SiO_2(RITC) is a synthesized MNP, consisting of a cobalt ferrite core ($CoFe_2O_4$) and silica shell, which contains chemically bound Rhodamine B isothiocyanate (RITC) as in our previous report.[25] Since cobalt ferrite core and RITC of MNPs@SiO_2(RITC) were included within the silica shell, chemical structure was stable at pH 2−3, and fluorescence was also preserved at 540 nm for a long period of time without photobleaching (data not shown). Previously, Kim *et al.* reported tissue distribution of MNPs@SiO_2(RITC) in mice and demonstrated that it traverses the blood−brain barrier (BBB) without inducing functional deficits.[9] In particular, human mesenchymal stem cells (hMSCs) labeled with MNPs@SiO_2(RITC) stably retained their properties without disturbances of surface phenotype or morphology.[12] Unfortunately, sufficient information was not provided to understand physiological and metabolic effect of MNPs@SiO_2(RITC) in previous reports.[9,12,25]

Here, we first investigated comprehensive changes following treatment with nanoparticles in cells using transcriptomic and metabolic studies. This approach included an evaluation of the effect of MNPs@SiO_2(RITC) on gene expression and metabolism, including AAs and OAs, through "systems biological analysis" combined with transcriptomic profiling analysis based on the Affymetrix oligo gene chip system for metabolite-related transcriptome profiles and metabolite profiling analysis based on gas chromatography−mass spectrometry (GC−MS). The results indicate that MNPs@SiO_2(RITC) can be used at optimal concentrations for diverse applications without disturbance of gene expression and metabolism.

RESULTS AND DISCUSSION

Analysis of Cytotoxicity and Cell Labeling Efficiency with MNPs@SiO_2(RITC). In a previous report, Park *et al.* determined that 0.1 μg/μL was the optimal concentration of MNPs@SiO_2(RITC) to attempt *in vitro* and MR imaging without toxicological effects in human cord blood-derived mesenchymal stem cells.[12] In addition, Kim *et al.* showed that 1.0 μg/μL of MNPs@SiO_2(RITC) has little effect on chromosome aberration in Chinese hamster lung fibroblast cells (CHL).[9] To evaluate cytotoxicity and cell labeling efficiency of MNPs@SiO_2(RITC) based on previous reports about concentrations of MNPs@SiO_2(RITC), we observed optical images for morphological changes of human embryo kidney (HEK) 293 cells treated with 0.01, 0.1, and 1.0 μg/μL of MNPs@SiO_2(RITC) for 12 h. Cells treated with these concentrations of MNPs@SiO_2(RITC) did not cause morphological changes, such as membrane or organelle destruction (Figure 1A). To determine the viability in response to treatment with two different concentrations of MNPs@SiO_2(RITC) (0.1 and 1.0 μg/μL) for 12 h, we labeled the samples with Annexin V and PI and then evaluated them by fluorescence-activated cell sorter (FACS) analysis (Figure 1B,C). The viability of cells was preserved at 99.34 and 98.69% for 0.1 and 1.0 μg/μL concentrations of MNPs@SiO_2(RITC), respectively. Compared to the nontreated control, FACS analysis showed no significant changes in the viability of MNPs@SiO_2(RITC)-treated cells. Furthermore, when MTS assays were conducted to assess the cytotoxic effect of MNPs@SiO_2(RITC) after 12 h or 3 or 7 days of treatment with 0.01−1.0 μg/μL, no significant cytotoxic effect was observed compared with nontreated control at the concentration/time combination tested (Supporting Information Figure S1). These results demonstrate that the viabilities of HEK 293 cells treated with MNPs@SiO_2(RITC) were not significantly different from those of the nontreated control, which concurs with previous reports.[9,12,25] These findings strongly suggest that cell growth and apoptosis are not significantly influenced by MNPs@SiO_2(RITC) at these concentrations.

For evaluation of the distribution and labeling efficiency of MNPs@SiO_2(RITC), HEK 293 cells were treated with three different concentrations of MNPs@SiO_2(RITC), and images were taken using confocal laser scanning microscopy (LSM). Labeled cells were detectable from a MNPs@SiO_2(RITC) concentration of 0.01 μg/μL, and labeling efficiency was increased dose-dependently (Supporting Information Figure S2). However, though labeling efficiency was increased in the 1.0 μg/μL MNPs@SiO_2(RITC)-treated group compared to the 0.01 μg/μL MNPs@SiO_2(RITC)-treated group, it was not dramatically increased when compared to the 0.1 μg/μL MNPs@SiO_2(RITC)-treated group, and cytoplasmic accumulations of aggregated MNPs@SiO_2(RITC) were also detected in HEK 293 cells treated with 1.0 μg/μL MNPs@SiO_2(RITC) (Supporting Information Figure S2 inset box).

Nanoparticle-related toxicity has been evaluated in terms of particle size, agglomeration, sedimentation, and diffusion as parameters of nanoparticle uptake.[26] In quantitative studies of the uptake of cerium oxide nanoparticles, small particles (25−50 nm) were almost transported by diffusion and agglomeration, while larger particles (250−500 nm) were transported by sedimentation. More specifically, the uptake of 20−50 nm nanoparticles did not occur singly, and their

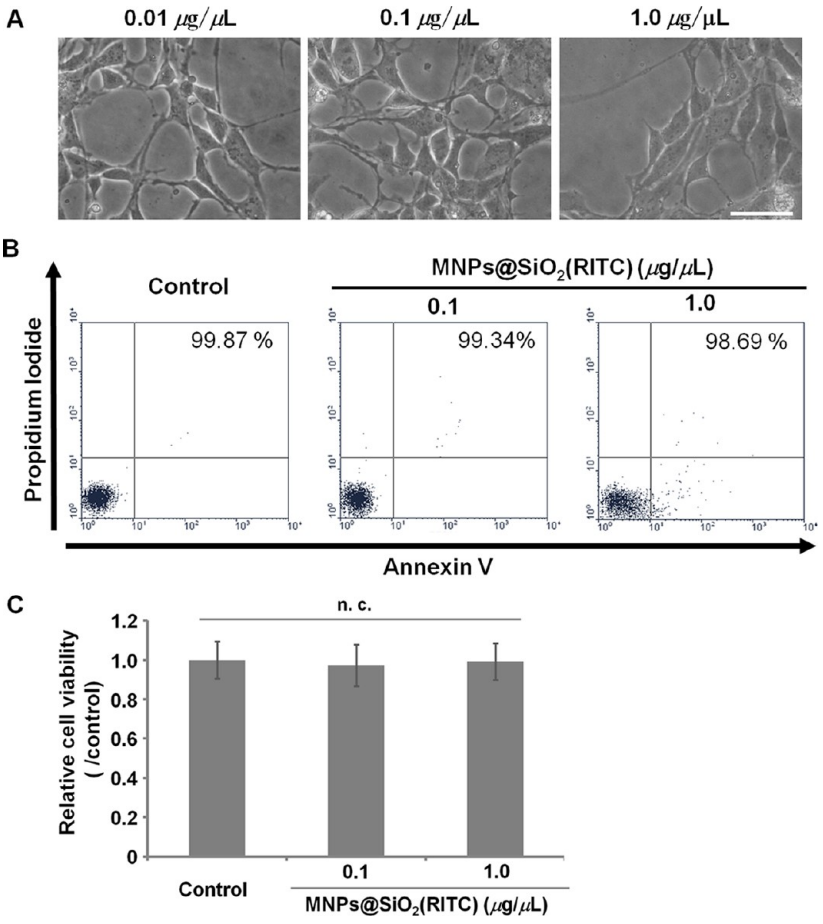

Figure 1. Optical microscopic appearance and FACS analysis for cell death in MNPs@SiO_2(RITC)-treated HEK 293 cells. HEK 293 cells were treated with 0.01, 0.1, and 1.0 μg/μL of MNPs@SiO_2(RITC) for 12 h. Micrographs of MNPs@SiO_2(RITC)-treated cells showed that significant cytotoxicity or morphological changes were not observed at these concentrations (A). HEK 293 cells were treated with 0.1 and 1.0 μg/μL of MNPs@SiO_2(RITC) for 12 h, followed by quantification of cell viability by FACS analysis after staining with Annexin V and propidium iodide (PI). These data were analyzed using Win MDI version 2.9. In all cases, cell viability was preserved at $\geq$95% (B). Images were taken at a magnification of 200$\times$, and scale bar indicates 150 μm. Data represent mean values of triplicates $\pm$ SD.

agglomeration was faster at higher concentrations. Therefore, we postulate that 50 nm MNPs@SiO_2(RITC) particles are transported primarily by diffusion and agglomeration; using confocal LSM, the agglomerated forms predominated in cells treated with 1.0 μg/μL MNPs@SiO_2(RITC) *versus* 0.1 μg/μL MNPs@SiO_2(RITC) (Supporting Information Figure S2). In addition, the uptake efficiency of MNPs@SiO_2(RITC) by HEK 293 cells was evaluated using a fluorescent assessment method in a fluorescence microplate reader (Molecular Devices, USA). After treatment of cells with 0.01−2.0 μg/μL MNPs@SiO_2(RITC) for 12 h, the MNPs@SiO_2(RITC) uptake increased with concentration, which is consistent with reports on cerium oxide and polymer NPs.[26,27] The uptake efficiency of MNPs@SiO_2(RITC) plateaued at 1.0 μg/μL (Supporting Information Figure S3). These results provided evidence to determine the maximum concentration of treatment. According to previous reports and our data, 0.1 and 1.0 μg/μL of MNPs@SiO_2-(RITC) were established as the low and high concentrations, respectively.

Gene Expression and AA Composition Profiling in MNPs@SiO_2-(RITC)-Treated HEK 293 Cells. For identification of genes upregulated and downregulated in MNPs@SiO_2(RITC)-treated HEK 293 cells, gene expression analysis was performed on HEK 293 cells treated with 0, 0.1, and 1.0 μg/μL of MNPs@SiO_2(RITC) using oligonucleotide microarrays. After normalization of gene expression, 5966 functional gene probes were classified into eight clusters using GenPlex 2.0 software (data not shown). Because clusters 1 and 3 represent significant signal changes, they were examined in further detail. Of the 466 functional genes in these clusters, 291 genes were either up- or downregulated at a MNPs@SiO_2(RITC) concentration of 1.0 μg/μL, using a 1.25-fold expressional change as a cutoff (Figure 2A). The signal intensities of total functional genes belonging to clusters 1 and 3 were plotted according to comparison between intensity levels of groups and then a comparison plot pattern could be separated into high and low differential expression (Figure 2B). Expressional difference between treated and nontreated cells was related

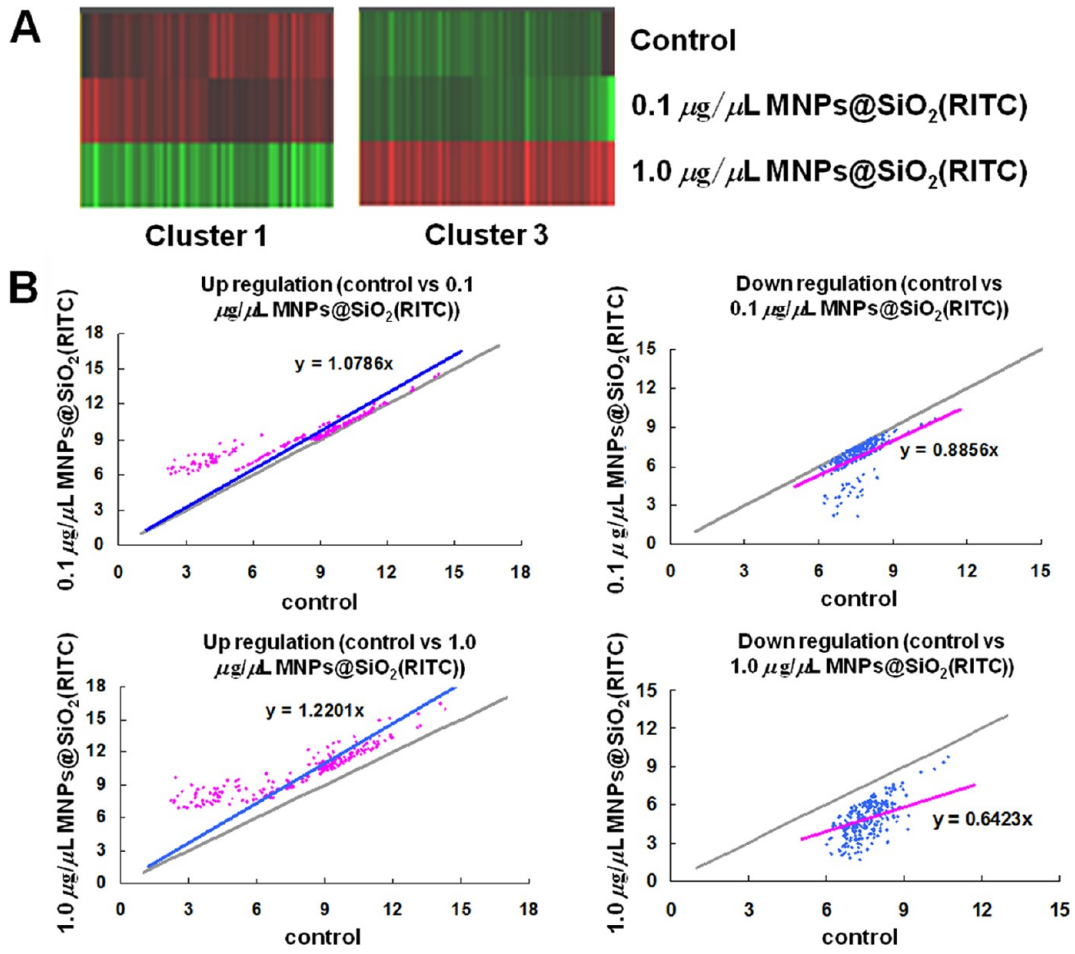

Figure 2. Clustering of gene expression and plotting of signal intensities in MNPs@SiO_2(RITC)-treated and nontreated cells; 2481 functional genes belonged to clusters 1 and 3; a dendrogram showed that 291 gene expressions changed by more than 1.25-fold; red, upregulated; green, downregulated (A). Correlation of expressional difference between control and MNPs@SiO_2(RITC)-treated HEK 293 cells. Signal intensities of all functional genes belonging to clusters 1 and 3 were plotted (B). The *X* and *Y* axes indicate the signal intensities of control and MNPs@SiO_2(RITC)-treated cells, respectively. The gray line indicates the criterion line which is standardized with nontreated control intensities.

to the concentration of MNPs@SiO_2(RITC). When 0.1 μg/μL MNPs@SiO_2(RITC)-treated cells was compared to the nontreated control, 7.8% of genes were upregulated and 1.4% were downregulated. However, when 1.0 μg/μL of MNPs@SiO_2(RITC) was administered, 22.0% of genes were upregulated and 35.8% were downregulated. We categorized genes with significantly changed expression after 1.0 μg/μL MNPs@SiO_2-(RITC) treatment, but not significantly changed after 0.1 μg/μL MNPs@SiO_2(RITC) treatment. Table 1 lists the functional categories of the 291 genes, including 205 upregulated and 86 downregulated genes after treatment with high concentrations (1.0 μg/μL) of MNPs@SiO_2(RITC).

Since metabolism-related genes were disturbed in high concentrations of the MNPs@SiO_2(RITC)-treated group (Table 1), we performed AA profiling analysis using our previous method.[28] The percentage composition of seven AAs from nontreated control, 0.1 μg/μL, and 1.0 μg/μL MNPs@SiO_2(RITC)-treated cells is shown in Table 2, and the values that were normalized to the mean level of the corresponding control group were used as variables to draw star graphs composed of seven rays; differences of control and treated groups were expressed as the visual star symbol plot (Figure 3). According to the percentage composition and normalized value of AAs, these clearly revealed a marked increase of glutamic acid (about 200%) and reduction ($\leq$30%) of other AAs (alanine, valine, leucine, isoleucine, proline, and tyrosine) in the group treated with 1.0 μg/μL of MNPs@SiO_2(RITC), while the group treated with 0.1 μg/μL of MNPs@SiO_2(RITC) showed slight changes (elevation or reduction, $\leq$20%) by comparison with those of the control group. The star symbol plot of the group treated with 1.0 μg/μL of MNPs@SiO_2-(RITC) was easily distinguishable from those of the control group and the group treated with 0.1 μg/μL of MNPs@SiO_2(RITC), while no large differences in the values of AAs between the control group and the group treated with 0.1 μg/μL of MNPs@SiO_2(RITC) were observed. Selected ion monitoring (SIM) chromatograms also revealed that glutamic acid was

significantly increased in the 1.0 μg/μL MNPs@SiO_2-(RITC)-treated group (Figure 4). In the SIM chromatograms, the relative peak area ratio of glutamic acid to that of the internal standard (IS) was 0.056 (Figure 4A; control), 0.045 (Figure 4B; treated with 0.1 μg/μL), and 0.173 (Figure 4C; treated with 1.0 μg/μL). In particular, glutamic acid levels in the group treated with 1.0 μg/μL of MNPs@SiO_2(RITC) were much higher than those of the control or 0.1 μg/μL MNPs@SiO_2(RITC)-treated groups. The branched-chain amino acids (BCAAs, such as valine, leucine, and isoleucine) play essential roles, including as a stimulators of the immune system and in the synthesis of glutamic acid; more than 30% of glutamic acids are derived from BCAAs through the BCAA transaminase pathway.[29−31] As shown in Table 2 and star symbol plots (Figure 3), alteration of BCAAs between high concentration MNPs@SiO_2(RITC)-treated cells and control was also observed, and these results provide a clue to the understanding of glutamic acid disturbance caused by high concentrations of MNPs@SiO_2(RITC).

TABLE 1. Categorization of Expression Changed Genes in High Dose MNPs@SiO_2(RITC)-Treated Condition

biological processing	upregulation	downregulation
DNA-related gene		
DNA replication and processing	6	nc[a]
DNA repair	3	1
transcription processing		
RNA polymerase II	9	3
regulation of transcription from RNA polymerase II	8	2
transcription	14	4
regulation of transcription	3	2
apoptosis	4	nc
transport		
cation, electron, and ion transport	12	11
protein transport	7	1
material transport	6	6
cell adhesion, motability, and cytoskeleton		
cell adhesion and movement	17	6
cell cytoskeleton	7	nc
signal		
intracellular signaling	8	1
cell to cell signaling	3	2
pathway and genesis signaling	11	14
protein process	17	6
ubiquitin relation	18	2
cell cycle, growth, development, and aging		
proliferation, differentiation, and development	6	1
cell cycle	7	3
cell growth and aging	5	nc
proliferation, differentiation, and development	9	8
cell metabolism	17	6

[a] No change.

Ingenuity Pathway Analysis (IPA) of the Glutamic Acid Metabolic Network in High Concentration MNPs@SiO_2(RITC)-Treated Cells. Since the GC−MS analysis result indicated that glutamic acid levels were elevated more than 2-fold in 1.0 μg/μL of MNPs@SiO_2(RITC)-treated cells compared to the control group, we constructed a genetic network of the glutamic acid metabolic pathway using Ingenuity pathway analysis (IPA) software to understand the interaction between differentially expressed genes and altered AA metabolites. The data set for differentially expressed genes by high concentration of MNPs@SiO_2(RITC) was adopted from microarray data ($p < 0.05$ and fold change >1.25), and the network of these genes was then constructed on the basis of their metabolic correlation. Figure 5 and Supporting Information Table S1 indicate that several genes can have direct involvement in the glutamic acid metabolic pathway, including aldehyde dehydrogenase 4 family member A1 (ALDH4A1), glutamic pyruvate transaminase 2 (GPT2), glutamate dehydrogenase 1 (GLUD1), glutamic oxaloacetic transaminase 2 (GOT2),

TABLE 2. Composition Percentage of Seven Amino Acids Found in Treated HEK 293 Cells with MNPs@SiO_2(RITC)

		composition[a]					
			MNPs@SiO_2(RITC)-treated group (n = 3)			normalized value[e]	
no.	amino acid	control (n = 3)	low concn (0.1 μg/μL)	high concn (1.0 μg/μL)	P value[d]	low concn	high concn
1	alanine	11.7 ± 0.2	9.6 ± 0.5 (0.001)[b]	9.9 ± <0.1 (0.00004)[c]	0.2	0.8	0.8
2	valine	9.2 ± 0.1	8.6 ± 0.2 (0.002)	6.4 ± 0.3 (0.00003)	0.0001	0.9	0.7
3	leucine	15.8 ± 0.1	15.7 ± 0.7 (0.4)	11.7 ± 0.7 (0.0003)	0.001	1.0	0.7
4	isoleucine	13.5 ± 0.1	12.4 ± 0.7 (0.03)	9.1 ± 0.6 (0.0001)	0.001	0.9	0.7
5	proline	6.1 ± 0.2	6.6 ± 0.3 (0.04)	4.8 ± 0.1 (0.0006)	0.0004	1.1	0.8
6	glutamic acid	19.0 ± 0.9	20.5 ± 1.6 (0.1)	37.5 ± 2.6 (0.0001)	0.0003	1.1	2.0
7	tyrosine	24.8 ± 0.9	26.6 ± 0.5 (0.02)	20.7 ± 0.9 (0.002)	0.0002	1.1	0.8

[a] Values as percentage of composition by each AA amount ratio to the total AA amount (ng/10^5 cells). [b] Student's t-test at 95% confidence level on the mean values of control group and treated group with MNPs@SiO_2(RITC) of 0.1 μg/μL. [c] Student's t-test at 95% confidence level on the mean values of control group and treated group with MNPs@SiO_2(RITC) of 1.0 μg/μL. [d] Student's t-test at 95% confidence level on the mean values between treated 0.1 μg/μL group and 1.0 μg/μL group with MNPs@SiO_2(RITC). [e] Normalized values of AAs in treated groups with MNPs@SiO_2(RITC) to corresponding mean values in the control group.

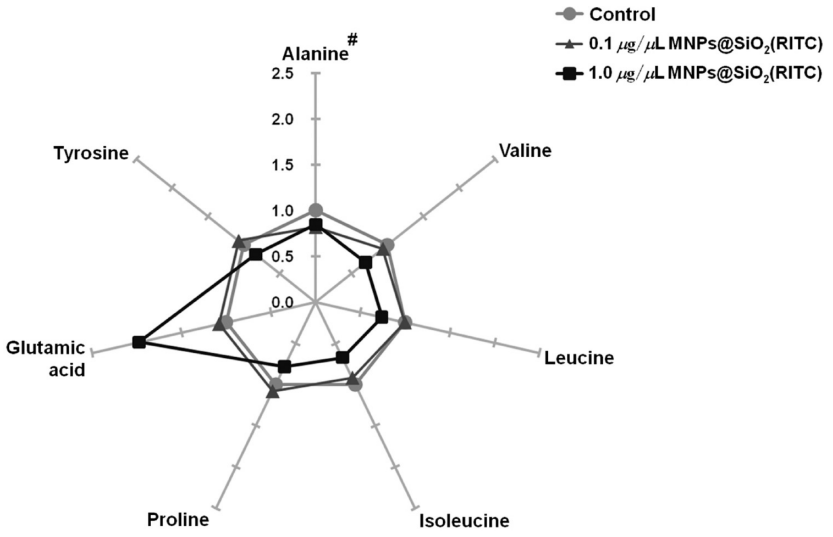

Figure 3. Star symbol plot of composition levels of the 7 AAs of nontreated HEK 293 cells and HEK 293 cells treated with MNPs@SiO_2(RITC). Star symbol plot of 0.1 and 1.0 μg/μL concentrations of MNPs@SiO_2(RITC)-treated cells based on the percentage mean composition levels of the 7 AA variables after normalization to the corresponding 7 AA mean values in the control group. The analysis was performed in triplicate and repeated independently (#, no significant change compared to control).

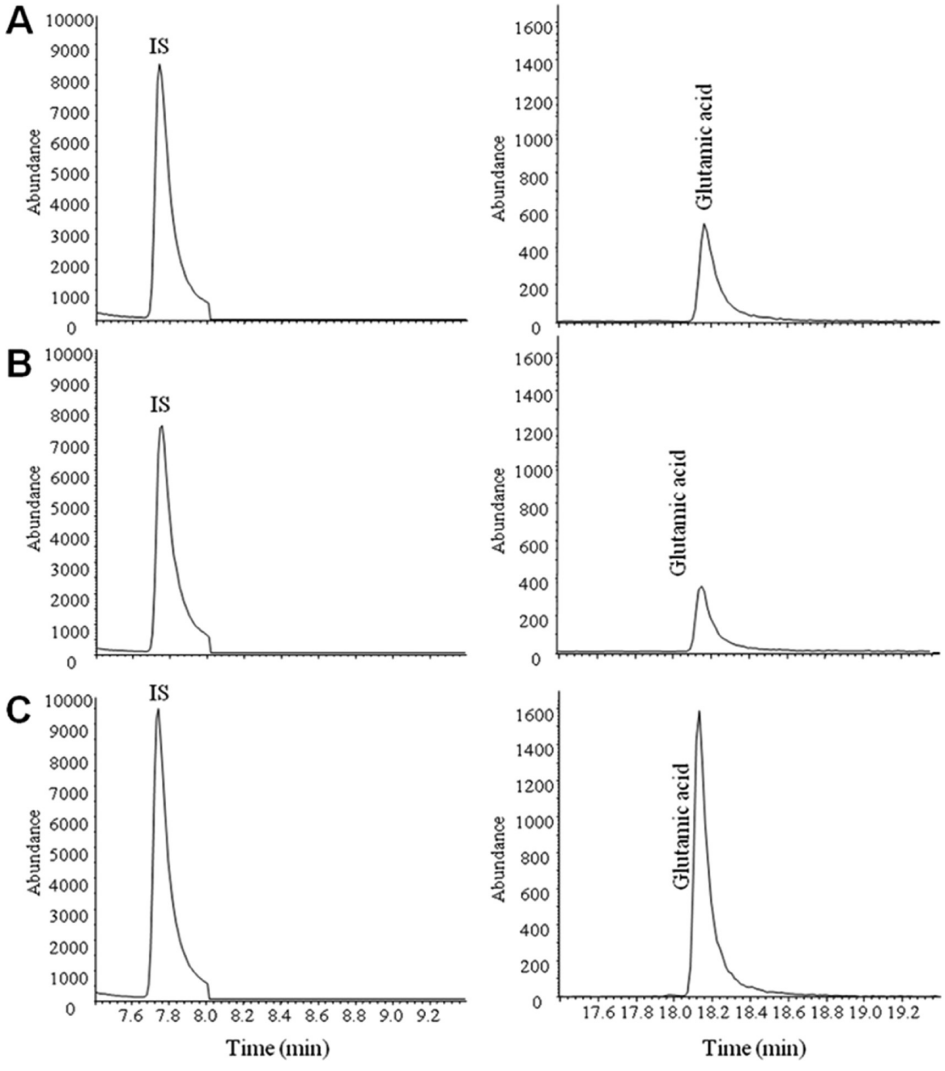

Figure 4. SIM chromatograms of glutamic acid in nontreated HEK 293 cells (A) and HEK 293 cells treated with MNPs@SiO_2-(RITC) of 0.1 (B), and 1.0 μg/μL (C). IS: Internal standard.

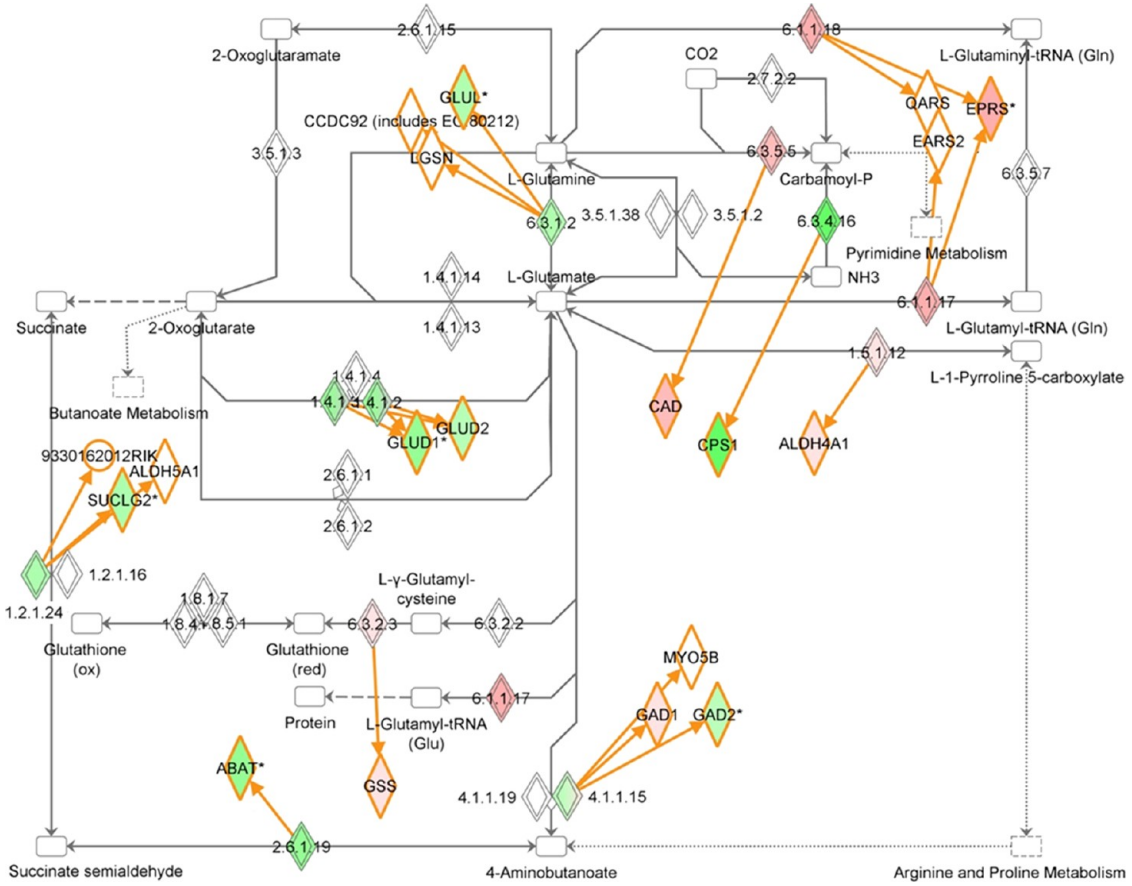

Figure 5. Glutamic acid pathways of significantly changed genes by MNPs@SiO_2(RITC) in microarray. The glutamic acid metabolic pathways presented here were constructed using IPA (version 8.5, Ingenuity Systems, http://www.ingenuity.com). The data set of differentially expressed genes adopted from microarray data with p values <0.05 and fold change >1.25. In representation of genetic networks, the red and green indicate up- and downregulated genes in cells treated with 1.0 μg/μL of MNPs@SiO_2(RITC), compared to control cells, respectively.

and glutamic acid decarboxylase 1 (GAD1), and can be disturbed in 1.0 μg/μL MNPs@SiO_2(RITC)-treated cells. These results suggest that disturbance of glutamic acid in cells treated with high concentrations of MNPs@SiO_2(RITC) might be caused by expression confusion of genes that are associated with the glutamic acid metabolic pathway as in microarray and IPA.

Analysis of Gene Expression Relative to Glutamic Acid Metabolism by Semiquantitative PCR. On the basis of significant changes in 1.0 μg/μL concentrations of MNPs@SiO_2(RITC)-treated cells in microarray and IPA, we approached evaluation of the expression level of the glutamic acid metabolic pathway related to these genes. Profiles of representative genes that can be involved in the metabolic pathway of glutamic acid are listed in Supporting Information Table S2. These genes that can be involved in catalysis of glutamic acid into the metabolic precursor or other amino acids, GLUD1, GOT2, GAD1, and GLUL, were downregulated in 1.0 μg/μL concentrations of MNPs@SiO_2(RITC)-treated cells (Figure 6A). In 1.0 μg/μL MNPs@SiO_2(RITC)-treated cells, expression of GLUD1 was 47% lower than that of the nontreated control. In addition, expression of GOT2, GLUL, and GAD1 were 33, 25, and 61% lower than that of nontreated controls, respectively, whereas cells treated with 0.1 μg/μL MNPs@SiO_2(RITC) did not show significant change. Conversely, GPT2 and ALDH4A1, known as glutamic acid synthetic transaminase which catalyze alanine and proline to glutamic acid through the transfer of an amino group from these amino acid degradation pathways, showed an approximately 41 and 53% increase in cells treated with 1.0 μg/μL MNPs@SiO_2(RITC), respectively (Figure 6B). Interestingly, GC–MS analysis results revealed that alanine and proline were significantly decreased, while glutamic acids were increased in high concentrations in MNPs@SiO_2(RITC)-treated cells. These results suggested that alanine and proline may be converted to glutamic acid by overexpressed GPT2 and ALDH4A1.

Determination of ROS Generation and Evaluation of Mitochondrial Matrix Disintegration in MNPs@SiO_2(RITC)-Treated Cells. Recently, several toxicity studies have focused on oxidative stress and the pro-inflammatory states induced by nanoparticles.[32−36] In fact, several have presented evidence that nanoparticles, including quantum dots and carbon nanotubes (CNTs), induce oxidative stress and a pro-inflammatory state.[37−39] In addition, silica particles could induce the generation of

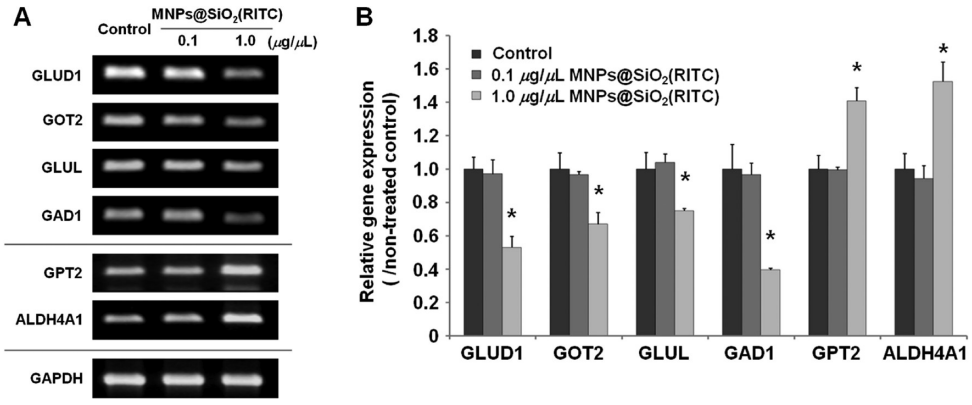

Figure 6. Quantitative evaluation of glutamic acid metabolic pathway related genes by RT-PCR and real-time PCR. Total RNA was reverse transcribed into cDNA, and 25 to 32 cycles PCR was performed using gene-specific primer pairs. PCR products were normalized *versus* GAPDH (internal control); GLUD1, glutamate dehydrogenase 1; GOT2, glutamic oxaloacetic transaminase 2; GLUL, glutamate ammonia ligase; GAD1, glutamic acid decarboxylase 1; GPT2, glutamic pyruvic transaminase 2; ALDH4A1, aldehyde dehydrogenase 4 family, member A1 (A). To quantify the transcriptomic changes of genes related to the glutamic acid metabolic pathway, real-time PCR was performed. GAPDH was used as the internal control. The histogram shows ratios of target genes, such as GLUD1, GOT2, GLUL, GAD1, GPT2, and ALDH4A1, normalized to corresponding means in the nontreated control (B); *$p < 0.05$, Student's *t*-test results at 95% confidence level were significantly different. The analysis was performed in triplicate and repeated independently.

intracellular reactive oxygen species (ROS) depending on the concentration of nanoparticles, and oxidative stress followed by ROS generation may cause damage to mitochondria and DNA.[40−44] We investigated whether MNPs@SiO_2(RITC) could induce the generation of intracellular ROS. 2′,7′-Dichlorodihydrofluorescin diacetate (DCFH-DA) staining was conducted to determine the generation of intracellular ROS induced by MNPs@SiO_2(RITC). An interesting result from this study is that ROS generation was observed in the group treated with a high concentration of MNPs@SiO_2(RITC), but ROS generation was not significant at a low concentration of MNPs@SiO_2(RITC). In confocal LSM images, 0.1 μg/μL of MNPs@SiO_2(RITC)-treated cells showed no significant difference in the ROS concentration compared to the nontreated control (Figure 7A). Interestingly, ROS were highly generated in cells treated with 1.0 μg/μL of MNPs@SiO_2(RITC), and we observed that ROS generation induced by MNPs@SiO_2(RITC) was concentrated in a cellular region in which MNPs@SiO_2(RITC) was accumulated. The ROS concentration, which was quantified with a fluorescence microplate reader, was significantly increased by more than 63% in cells treated with 1.0 μg/μL of MNPs@SiO_2(RITC) *versus* the nontreated control, while no significant differences between the control group and the group treated with 0.1 μg/μL of MNPs@SiO_2-(RITC) were observed (Figure 7B).

Previously, Park *et al.* reported that the level of ROS in the RAW264.7 group treated with 40 ppm silica NPs increased by 139.1% compared with the nontreated control group.[34] In our study, the increase of ROS in cells treated with 1000 ppm (1.0 μg/μL) MNPs was 163% of the nontreated control. Although the MNP concentration was 25 times that in the previous report, the ROS concentration increased by just 24% in our experiment. We postulate that this resulted from the fact that the treatment time with MNPs was only 12 h in our study *versus* 24 h using silica NPs in the previous report.

To investigate whether the intracellular ROS were generated by the silica shell or cobalt ferrite core, we evaluated ROS generation after treatment with 50 nm engineered silica NPs. These consisted of a solid silica shell (SiO_2) doped with the fluorescent dye Rhodamine B and metals with similar concentrations of $FeCl_3 \cdot 6H_2O$, $CoCl_2 \cdot 6H_2O$, and $Fe(NO_3)_3 \cdot 9H_2O$ in the cobalt ferrite core ($CoFe_2O_4$).[45] In addition, 50 nm Fe_2O_3 particles were added to adjust the particle size. The concentrations of each metal were determined based on the diameter of the cobalt ferrite core (9 nm), the density of MNPs@SiO_2(RITC) (2.2 μg/mm^3), and the density of the cobalt ferrite core (5.3 μg/mm^3).[25] When cells were treated with 0.1 or 1.0 μg/μL silica NPs, the amount of ROS generated and the confocal LSM images gave similar results as those of the MNPs@SiO_2-(RITC) at each concentration (Supporting Information Figures S4 and S5), while the core metals induced notably high levels of ROS generation and cell death at each concentration used. These data provide sufficient evidence to infer that the generation of intracellular ROS is caused by the accumulation of aggregated MNPs@SiO_2(RITC), and the silica shell, not the cobalt ferrite core, of the MNPs@SiO_2(RITC) is the main factor leading to intracellular ROS production. This is consistent with reports that silica-coated MNPs protected cells from oxidative stress by preventing soluble iron mobilization or acidic erosion.[9,46]

The mitogen-activated protein kinase (MAPK) pathway, known as the oxidative stress signal pathway followed by ROS, showed gene expression differences of approximately 40% in the group treated with a high

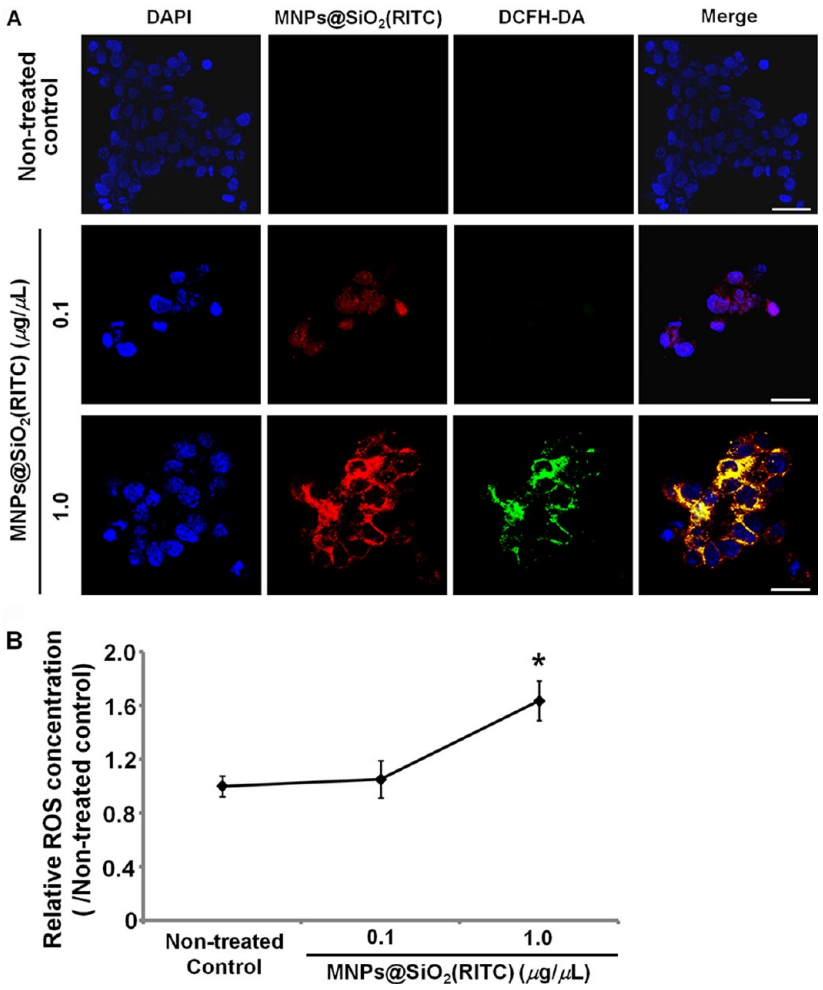

Figure 7. Intracellular ROS generation of HEK 293 cells after treatment with MNPs@SiO_2(RITC). To evaluate the generation of ROS, confocal microscopy images obtained from nontreated HEK 293, 0.1, and 1.0 μg/μL MNPs@SiO_2(RITC)-treated HEK 293 cells using DCFH-DA staining method (A). These samples were excited at 480 nm, and the emission signal was collected at 530 nm. Images were taken at a magnification of 200×, and scale bar indicates 100 μm. Blue, DAPI; red, MNPs@SiO_2(RITC); green, DCFH-DA. The merged image indicates that ROS distribution overlaps with the MNPs@SiO_2(RITC) localized region. To measure the concentration of ROS, DCFH-DA stained cells were quantified with a fluorescence microplate reader at 480/530 nm (excitation/emission), and intensities were normalized to a nontreated control (B). The intensity of non-oxidized DCFH-DA was used as a blank standard, and data represent mean values of quintuples ± SD; *$p < 0.05$, Student's t-test results at 95% confidence level were significantly different.

concentration of MNPs@SiO_2(RITC) compared to the nontreated control (data not shown). However, the cell death induced by oxidative stress was not observed with a high concentration of MNPs@SiO_2(RITC). Thus, we assume two causes for these phenomena: (i) MNPs@SiO_2(RITC) treatment time (12 h) was not sufficient to trigger the apoptosis pathway followed by oxidative stress, and (ii) the distribution of generated ROS is restricted to the cellular region with accumulated MNPs@SiO_2(RITC) without diffusion into the whole of the cell. In addition, the increased glutamic acid level due to MNPs@SiO_2(RITC) might serve as an antioxidant because it induces increased antioxidant levels to assist detoxification.[47] We postulated that increased glutamate partly contributes to ameliorating the elevated ROS levels in mitochondria since it had no effect on cell viability due to MNPs@SiO_2(RITC) as determined by the FACS (Figure 1B,C) and MTS assay (Supporting Information Figure S1). Further studies are needed to elucidate the correct reason for these phenomena in cells treated with a high concentration of MNPs@SiO_2(RITC) since we could not accumulate sufficient data about the long-term treatment of MNPs@SiO_2(RITC) on cells and the inflammatory reaction mediated by ROS that is generated by a high concentration of MNPs@SiO_2(RITC).

Alteration of ATP Synthesis and Composition of OAs That Are Relative to the Krebs Cycle in MNPs@SiO_2(RITC)-Treated Cells. Several studies have suggested that cellular regulation of glutamic acid metabolism was decisively affected by the mitochondrial membrane potential because the principal genes for glutamic acid metabolism, including GLUL, GAD1, and ALDH4A1, are functionalized as mitochondrial matrix enzymes.[48−54] Furthermore, several studies have also suggested that mitochondrial damage was induced by nanoparticles

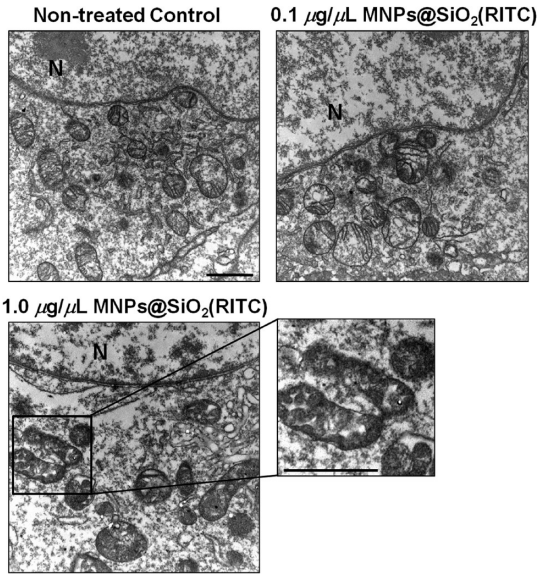

Figure 8. TEM images of mitochondria in HEK 293 cells treated with MNPs@SiO_2(RITC). Inner structures of mitochondria were disintegrated in cells treated with a high concentration of MNPs@SiO_2(RITC) (arrow), whereas mitochondria of nontreated control and 0.1 μg/μL MNPs@SiO_2(RITC)-treated cells contained complex structures of the inner membrane. The mitochondria morphology was obtained from independent triplicate assessment using TEM at a magnification of 25 000× and 75 000× (small box). N, nucleus.

through the oxidative stress mechanism followed by ROS.[55,56] Accordingly, we hypothesized that disturbance of gene expression and generation of ROS induced by MNPs@SiO_2(RITC) can effect mitochondrial disorder including structure disintegration and depolarization and assessed mitochondria with transmission electron microscopic (TEM) and the JC-1 assay kit (Molecular Probe, USA) according to the manufacturer's protocol and the previous report.[57] Interestingly, TEM images and JC-1 assay revealed that mitochondrial inner structures were disintegrated, and mitochondrial membranes were depolarized in cells treated with high concentrations of MNPs@SiO_2(RITC). As shown in Figure 8, cells treated with 1.0 μg/μL of MNPs@SiO_2(RITC) exhibited altered mitochondria, with an irregular, disintegrated inner structure, whereas the mitochondria of nontreated control cells retained the complex structures of the inner mitochondrial membrane; the mitochondrial structure of 0.1 μg/μL MNPs@SiO_2(RITC)-treated cells was similar to that of control cells. Furthermore, confocal LSM images indicated that treatment with 1.0 μg/μL of MNPs@SiO_2(RITC) could result in mitochondrial depolarization, although the cells show no significant gross morphological changes (Supporting Information Figure S6). Conversely, the mitochondrial depolarization of cells that were treated with 0.1 μg/μL of MNPs@SiO_2(RITC) was similar to that of nontreated control cells. Previous reports demonstrated that several nanoparticles, such as nanosilver and hydroxyapatite particles, induce mitochondria-dependent apoptotic cell death through oxidative stress and a mitochondrial depolarization pathway.[58,59] Although these results showed structural disintegration and depolarization in mitochondria following MNPs@SiO_2(RITC) treatment, we could not observe mitochondria-dependent apoptotic cell death induced by MNPs@SiO_2(RITC), and the microarray result also indicated no significant changes of apoptotic cell death related genes (data not shown). These phenomena demonstrate that structural disintegration and depolarization in mitochondria following MNPs@SiO_2(RITC) treatment are not sufficient to induce mitochondria-dependent apoptosis or significant changes in apoptosis-related genes. However, further investigation is necessary to understand the cascade of the MNPs@SiO_2(RITC) effect on the mitochondrial membrane potential.

The Krebs cycle is a mainstream of ATP generation in mitochondria and involves catalytic enzyme reactions of OAs, including acetyl-CoA, citrate, fumarate, malate, and oxaloacetate.[22] Since these results provide evidence that a high concentration of MNPs@SiO_2(RITC) may have the potential to affect mitochondrial function through generation of ROS, the effect of MNPs@SiO_2(RITC) on the process of ATP synthesis was evaluated with a luminescence-based ATP concentration assay system. When 1.0 μg/μL MNPs@SiO_2(RITC)-treated cells were compared to nontreated controls, the ATP concentration was dramatically decreased, whereas 0.1 μg/μL MNPs@SiO_2(RITC)-treated cells showed no significant difference compared to nontreated controls (Figure 9A). In addition, the ATP concentration, which was quantitatively evaluated by luminescence images, showed a significant reduction of approximately 50% in 1.0 μg/μL MNPs@SiO_2(RITC)-treated cells *versus* the nontreated control (Figure 9B). However, there was no significant difference in the ATP concentration between the nontreated control and 0.1 μg/μL MNPs@SiO_2(RITC)-treated cells. These results indicate that disintegration of the mitochondrial inner structure, which is induced by high concentration treatment with MNPs@SiO_2(RITC), also affects mitochondria function including ATP synthesis; however, it does not significantly change after treatment with low concentration MNPs@SiO_2(RITC). When the overall mitochondrial metabolism was evaluated using the MTS assay for 12 h or 3 or 7 days, no significant changes were observed for MNPs@SiO_2(RITC) concentrations from 0.01 to 1.0 μg/μL (Supporting Information Figure S1). Although ATP generation was reduced by approximately 50% compared to the nontreated control group in this study, the changes in reductase in the Krebs cycle were not sufficiently reflected in the MTS assay because it evaluates the total reductase activity in cells, rather than that of the Krebs cycle only.[60]

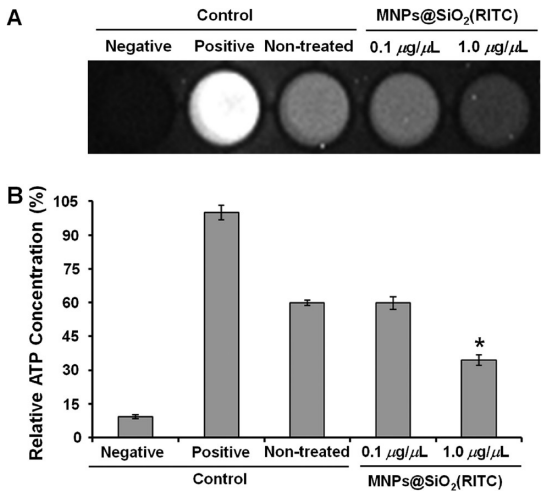

Figure 9. Reduction of ATP generation activity in HEK 293 cells treated with MNPs@SiO_2(RITC). A luminescence-based assay was performed on nontreated, 0.1 μg/μL, and 1.0 μg/μL MNPs@SiO_2(RITC)-treated HEK 293 cells using an ATP concentration assay system (A). The ATP concentration, which was evaluated by luminescent images, was significantly decreased in the 1.0 μg/μL MNPs@SiO_2(RITC)-treated group compared to the nontreated or 0.1 μg/μL MNPs@SiO_2(RITC)-treated group (B). The intensities were quantified with MultiGauge 3.0 software, and data represent mean values related to the positive control of triplicate ± SD; *$p < 0.05$, Student's *t*-test results at 95% confidence level were significantly different.

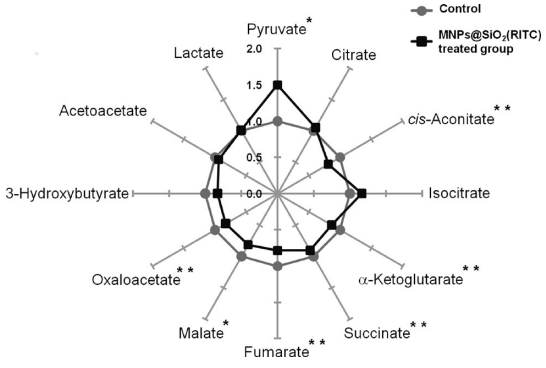

Figure 10. Star symbol plot of composition levels of the 12 OAs of nontreated HEK 293 cells and MNPs@SiO_2(RITC)-treated HEK 293 cells. Star symbol plot of 1.0 μg/μL MNPs@SiO_2(RITC)-treated cells based on the percentage mean composition levels of the 12 OAs after normalization to the corresponding mean values of the 12 OAs in the control group; *$p < 0.05$, **$p < 0.01$, Student's *t*-test results at 95% confidence level were significantly different.

Since OAs play an important role in the Krebs cycle of mitochondria in terms of ATP generation, we investigated alteration of OAs, including pyruvate, α-ketoglutarate, and oxaloacetate, using our previous method.[61] As shown in Figure 10 and Supporting Information Table S3, the composition of OAs, which are metabolites produced by the Krebs cycle, was observed as having significant variation in MNPs@SiO_2-(RITC)-treated cells compared to the nontreated control group. In particular, pyruvate of the MNPs@-SiO_2(RITC)-treated group was markedly elevated by more than 50%, while α-ketoglutarate and oxaloacetate were significantly reduced by 17 and 14%, respectively, compared to the nontreated control group. In addition, other OAs in the Krebs cycle, such as fumarate and malate, were also decreased in cells treated with a high concentration of MNPs@SiO_2(RITC). Since these OAs are also converted by transaminase of glutamic acid such as GPT2, GOT2, and GLUD1, alteration of OAs was explained by disturbance of transaminase induced by high concentration MNPs@SiO_2(RITC). Taken together with the ATP level of the group treated with a high concentration of MNPs@SiO_2(RITC), compositional changes of OAs demonstrate that the alteration of ATP synthesis is caused by a disturbance of the Krebs cycle induced by a high concentration of MNPs@SiO_2-(RITC). In a previous study, Lu *et al.* reported that the AAs and energy metabolism involving Krebs cycle intermediates were disturbed in silica NPs using an *in vivo* model, which is similar to our metabolic data.[62] They also demonstrated that the surface area of silica NP-related reactive chemical stress affected the toxicity, followed by a dose-dependent accumulation of NPs. On the basis of these results, we hypothesized that reactive chemical stress followed by MNPs@SiO_2-(RITC) accumulation may be the fundamental cause of MNPs@SiO_2(RITC)-induced metabolic dysfunction. Further research is needed to clarify comparable stresses that induce similar metabolic profile changes to understand the physicochemical properties of nanomaterials in biological systems.

Beck *et al.* demonstrated that the biological activity of bone cells was stimulated at silica NP concentrations ≤0.1 μg/mL; these were identical to the MNPs@SiO_2-(RITC), except they lack a cobalt ferrite core.[45] Although the silica NPs had anti-osteoclastogenic activity at ≤0.1 μg/mL in the murine monocytic cell line RAW264.7, the silica NP dose range (0.01−0.1 μg/mL) exhibited no toxic effect on the cells after 10 days, which is consistent with Supporting Information Figure S1 and previous reports.[10,45] Therefore, we postulated that silica NPs have osteoclastogenic activity at 0.1 μg/mL due to the small changes in the transcriptome profile, as seen in cells treated with 0.1 μg/mL of MNPs@SiO_2(RITC) (Figure 2), and have more marked effects on cell differentiation than viability.

There are several limitations to our study. First, although kidney tissue is known to be one of the main tissues in which nanomaterials accumulate, our present study is restricted to use of kidney-derived cells treated with MNPs@SiO_2(RITC). Furthermore, the cellular responses to nanoparticles are poorly understood and are controversial because different cell types appear to have different responses and concentration sensitivities.[63−65] Therefore, further studies must examine the effect of nanoparticles on various cell types before drawing conclusions regarding their suitability for biomedical applications. Second, we evaluated the

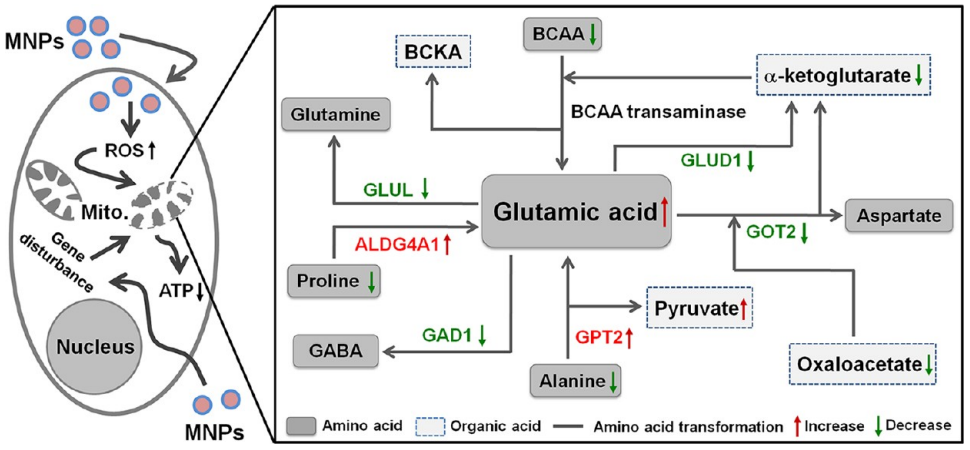

Figure 11. Schematic pathways of the cellular events and glutamic acid disturbance in cells treated with a high concentration of MNPs@SiO_2(RITC). This illustration indicates the cellular event that occurred after treatment with a high concentration of MNPs@SiO_2(RITC). A high concentration of MNPs@SiO_2(RITC)-induced mitochondrial dysfunction through generation of ROS and disturbance of genes relative to the glutamic acid metabolic pathway. Downregulation of genes, such as GLUD1, GLUL, GOT2, and GAD1, prevents catalysis of glutamic acid into its precursor or other amino acids, while upregulation of GPT2 and ALDH4A1 involves conversion of other amino acids to glutamic acid. Consequently, glutamic acid may be increased according to this complicated interaction of cellular events and gene expression, while alanine, proline, and BCAAs are reduced. Our structured model was predicated upon confirmed transcriptomic and metabolic data.

alteration of gene expression and metabolism in cells after only 12 h of treatment with MNPs@SiO_2(RITC). Additional studies are needed that concern the time-related impact of MNPs@SiO_2(RITC) for better understanding of the late effect of nanoparticles on gene expression and metabolic difference. Lastly, we suggested that the generation of ROS is a crucial cause of mitochondrial dysfunction in the group treated with a high concentration of MNPs@SiO_2(RITC). Further studies concerning the mechanism of ROS generation induced by a high concentration of MNPs@SiO_2(RITC) including the stability of silica shell and the distribution in cellular organelles are needed.

CONCLUSION

To the best of our knowledge, this work is the first systems biological study to attempt cytotoxicological evaluation of nanoparticles. The present study shows that high concentrations of MNPs@SiO_2(RITC) affect gene expression and metabolism in HEK 293 cells. In addition, we found that a high concentration of MNPs@SiO_2(RITC) could induce mitochondrial dysfunction through disturbance of related genes and generation of intracellular ROS. On the basis of data obtained from our present study, the processes of cellular events induced by a high concentration of MNPs@SiO_2(RITC) were proposed: (i) treatment with high concentration of MNPs@SiO_2(RITC), (ii) related gene and metabolite disturbance, (iii) production of ROS, (iv) damage of mitochondria, (v) disorder of cellular process (*i.e.*, Krebs cycle), and (vi) reduction of ATP generation. The comprehensive strategy is illustrated in Figure 11, and we demonstrate that high concentrations of MNPs@SiO_2(RITC) can lead to disturbance in cellular metabolism, such as the metabolism of glutamic acid and its precursors, through induction of expressional disturbance of metabolic pathway related genes and mitochondrial dysfunction followed by ROS, although MNPs@SiO_2(RITC) are not directly cytotoxic to the treated cell.

In this present study, we demonstrate that an overdose (1.0 μg/μL) of MNPs@SiO_2(RITC) can be a cause of transcriptomic and metabolic disturbance; however, it can be used at concentrations considered optimal for biomedical application without inducing undue cytotoxicity. Further studies are required to investigate the implications of accumulation mechanisms and perturbation of a variety of metabolites and genes by MNPs@SiO_2(RITC).

MATERIALS AND METHODS

Cell Culture and MNPs@SiO_2(RITC) Treatment. Human embryo kidney 293 (HEK 293) cells were used to evaluate the cytotoxicity of MNPs@SiO_2(RITC) because this cell line has been well-characterized for its relevance to silica nanoparticle-induced cytotoxicity and the eventual renal toxicity models in human.[66,67] Cells were cultured in high glucose Dulbecco's modified Eagle's medium (DMEM, Gibco, USA) containing 10% fetal bovine serum (FBS, Gibco, USA), 100 units/mL penicillin, and 100 μg/mL streptomycin (Gibco, USA). Cells were incubated at 37 °C in a 5% humidified CO_2 atmosphere. Media were removed and replaced every 3 days. MNPs@SiO_2(RITC) particles of 50 nm diameter were added directly to serum and antibiotic-free culture medium. HEK 293 cells were seeded with 2×10^6 cells/100 mm dish and incubated in 10 mL of medium containing various concentrations of MNPs@SiO_2(RITC) for 12 h. Cells were then washed twice in phosphate buffered saline (PBS) and harvested using 0.25% trypsin/0.1% EDTA (Sigma, USA).

Fluorescence-Activated Cell Sorting (FACS) Analysis. For cell death assays, FACS analysis was performed using an Annexin V-FITC

apoptosis detection kit (Becton Dickinson Biosciences, USA) according to the manufacturer's protocol. Briefly, cells were harvested and then washed with cold PBS twice, after which they were resuspended in 100 μL of 1× binding buffer (10 mM Hepes, pH 7.4, 140 mM sodium chloride, and 2.5 mM calcium chloride). Then, 5 μL of Annexin V-FITC and propidium iodide (PI) was added to the samples, which were incubated for 15 min at 25 °C in the dark. To stop the reaction, 400 μL of 1× binding buffer was added to each tube. Cells were assayed by FACS (Becton Dickinson Facsvantage, USA), and data analysis was performed with Win MDI Version 2.9 (The Scripps Research Institute, USA).

Confocal Laser Scanning Microscopy (LSM) and Image Processing. MNPs@SiO_2(RITC)-treated HEK 293 cells were fixed in 4% paraformaldehyde solution, dehydrated, and mounted using antifade solution (R&D, USA). Cells were also 4′,6-diamidino-2-phenylindole (DAPI) stained for detection of nuclei. Fluorescence images were acquired by confocal LSM (Olympus, Japan). DAPI and MNPs@SiO_2(RITC) were excited at 405 and 530 nm wavelength using laser light, respectively. Digital images were analyzed using LSM software (Leica, USA).

RNA Purification with RNAzol B. RNA was isolated from MNPs@SiO_2(RITC)-treated or nontreated HEK 293 cells using RNAzol B (Tel-Test, Inc., USA) and then purified using RNeasy Mini Kits (Qiagen, USA) according to the manufacturer's instructions. Briefly, harvested cells were treated with 1 mL of RNAzol B. Chloroform was added, and then cells were incubated at 4 °C for 5 min. Total RNA was precipitated with 600 μL of isopropyl alcohol, and RNA pellets were washed with 70% ethanol. RNA was eluted from pellets using RNase-free water (WelGene, South Korea). RNA was quantified by spectrophotometry (Eppendorf, USA) and agarose gel electrophoresis. The purity of the RNA used for the microarray and PCR experiments ranged from 1.9 to 2.0, based on the ratio of optical densities (OD) at 260/230 and 260/280.

Quantitative Reverse Transcription PCR (RT-PCR) and Real-Time PCR. To quantify expression of genes, total RNA samples were reverse-transcribed using the ImProm-II reverse transcription system (Promega, USA), according to the manufacturer's instructions, and amplified using gene-specific primer pairs. PCR reactions were run in triplicate, and results were averaged. Gene-specific primers for RT-PCR conformation are listed in Supporting Information Table S4. To remove template errors, PCR products were normalized *versus* glyceraldehyde-3-phosphate dehydrogenase (GAPDH) PCR products amplified from the same samples. Amplified PCR products were separated on 1% agarose gels and stained with ethidium bromide. Amplified PCR product quantities were calculated and normalized using Multi Gauge 3.0 software (Fujifilm, Japan). The expression levels of glutamic-acid-related genes was determined using the RealMOD SYBR Green real-time PCR kit (iNtRON Biotechnology, Seongnam, South Korea) and DNA Engine (Bio-Rad, Hercules, CA), with gene-specific primer pairs (Supporting Information Table S5). The reactions were carried out at 5 °C for 2 min, 95 °C for 30 s, followed by 41 cycles of 95 °C for 5 s and 57 °C for 30 s, according to the manufacturer's protocol. The threshold cycle (C_t) value was determined as the point at which fluorescence significantly above the background level was detected, and the PCR products were analyzed by generating a melting curve using MJ Opticon Monitor Version 3.1 (Bio-Rad, Hercules, CA). The relative quantification of gene expression was performed using the 2^{-ddCt} method.[68] The PCR reactions were run in triplicate and repeated independently.

Microarray Experiments and Data Analysis. For construction of the gene expression profile, total RNA was hybridized to a microarray gene chip (Affymetrix, USA), according to the manufacturer's instructions. Briefly, the Affymetrix system (Beyond Bioinformatics ISTECH AATC) Human U133 Plus 2.0 50 K microarray, which contained 54 675 gene-specific probes, was used. Hybridization was performed overnight using 15 μg of labeled RNA product. After hybridization, these arrays were washed several times and scanned using Affymetrix scanners. Pretreatment was performed using GCOS, global scaling in GenPlex 3.0 software (ISTECH, South Korea). Gene expression differences were confirmed using MA plot with control cells and experimental arrays. For identification of pathways and functional networks, data sets of significantly changed genes were uploaded to Ingenuity Pathway Analysis (IPA version 8.5, Ingenuity Systems, http://www.ingenuity.com), which is a Web-based bioinformatics software for identification of biological functions and pathways from the IPA knowledge database constructed through scientific publications and literature. Data sets for significantly changed genes were generated using a 1.25-fold expressional change as a cutoff.

Chemicals and Reagents for AA and OA Profiling Analyses. AA standards, norvaline as an internal standard (IS) for AA analysis, OA standards, 3,4-dimethoxybenzoic as IS for OA analysis, methoxyamine hydrochloride, triethylamine, and ethyl chloroformate (ECF) were purchased from Sigma-Aldrich (USA). *N*-Methyl-*N*-(*tert*-butyldimethylsilyl)trifluoroacetamide (MTBSTFA) was obtained from Pierce (Rockford, USA). Toluene, diethyl ether, and ethyl acetate, including dichloromethane as pesticide-grade, were purchased from Kanto Chemical (Japan). Sodium hydroxide and sulfuric acid were purchased from Duksan (South Korea).

Sample Preparation for AA Profiling Analysis in Cells. AAs in nontreated HEK 293 cells (control group) and HEK 293 cells treated with MNPs (treated group) at concentrations of 0.1 and 1.0 μg/μL following cell lysis were identified by GC−MS in selected ion monitoring (SIM) mode after ethoxycarbonyl (EOC)/*tert*-butyldimethylsilyl (TBDMS) derivatives, as in our previous report.[28] Briefly, aliquots of each group (1×10^5 cells) were adjusted to pH ≥ 12 after addition of IS (200 ng). A two-phase EOC reaction was performed in the aqueous phase by vortexing for 5 min with ECF (20 μL) in the dichloromethane phase (1 mL). The reaction mixture was sequentially extracted with diethyl ether (3.0 mL) and ethyl acetate (2.0 mL), which were evaporated to dryness under a gentle nitrogen stream (40 °C). The residue was reacted (60 °C for 30 min) with MTBSTFA (20 μL) in toluene (20 μL) for GC−SIM−MS.

Gas Chromatography−Mass Spectrometry. GC−MS analyses in both scan and SIM modes were performed using an Agilent 6890N gas chromatograph, interfaced with an Agilent 5975B mass-selective detector (70 eV, electron impact mode) and installed with an Ultra-2 (5% phenyl/95% methylpolysiloxane bonded phase; 25 m × 0.20 mm i.d., 0.11 μm film thickness) cross-linked capillary column (Agilent Technologies, USA), as in our previous reports.[69,70] Temperatures of injector, interface, and ion source were 260, 300, and 230 °C, respectively. Helium was used as the carrier gas at a flow rate of 0.5 mL/min with constant flow mode. Samples were introduced in the split-injection mode (10:1). The oven temperature for AA analysis was initially set at 140 °C (2 min) and increased first to 240 at 5 °C/min and then to 300 °C (3 min) at 30 °C/min as in our previous report.[28] The oven temperature for OA analysis was initially set at 100 °C (2 min) and increased first to 250 at 5 °C/min and then to 300 °C (5 min) at 20 °C/min as in our previous report.[61] The mass range scanned was 50−600 u at a rate of 0.99 scans/s. In the SIM mode, three characteristic ions for each AA were used for peak identification and quantification.

Star Symbol Plotting. The amount of each AAs and OAs in cells of control and treated groups was determined based on calibration curves, which were then converted into percentage composition. AAs and OAs levels in cells of each group were normalized to the corresponding means in the control group. Subsequently, each normalized value was plotted as a line radiating from a common central point, and the far ends of the lines were joined together to produce star patterns using MS Excel, as described elsewhere.[61]

Transmission Electron Microscopic Observation. The cells were harvested using trypsin/EDTA and washed with PBS twice. Cells were then fixed with Karnovsky's fixative solution (1% paraformaldehyde, 2% glutaraldehyde, and 2 mM calcium chloride) for 48 h and washed with cacodylate buffer.[71] For postfixation, the cells were incubated in 1% osmium tetroxide (OsO_4) solution containing 0.05% potassium ferrocyanide ($K_4Fe(CN)_6$) for 90 min. Subsequently, cells were sectioned using Reichert Jung Ultracul S (Leica, USA). After the cells were stained with uranyl acetate and lead citrate, they were observed and photographed under TEM (JEM-1400, JEOL Ltd., Japan). Images were obtained

at 25 000× magnification in randomly chosen fields from several samples.

Measurement of Reactive Oxygen Species (ROS). The level of intracellular ROS was evaluated by 2′,7′-dichlorodihydrofluorescein diacetate (DCFH-DA) dye according to the manufacturer's protocol (Cell Biolabs, USA). Briefly, 1×10^4 and 2×10^4 cells were seeded in chamber slides and a black 96-well plate, respectively, and treated with MNPs@SiO_2(RITC) (0.1 and 1.0 μg/μL) for 12 h. After the medium was discarded, cells were washed with PBS twice. Then, 1× DCFH-DA/media solution was added to each well, and the cells were incubated at 37 °C for 1 h. These samples were washed with PBS twice, and fluorescence was measured using confocal LSM (Olympus, Japan) and Gemini EM fluorescence microplate reader (Molecular Devices, USA) at 480 nm excitation/530 nm emission. For detection of nuclei with confocal LSM, cells were stained with DAPI.

Measurement of the Adenosine Triphosphate (ATP) Concentration. The ATP concentration of cells was measured using an ATP assay system (Promega, USA) according to the manufacturer's protocol. Briefly, cells were harvested using 0.25% trypsin/0.1% EDTA and washed with PBS twice. To extract ATP without degradation, the harvested cells were resuspended in 0.1% trichloroacetic acid (TCA, Sigma, USA) solution and incubated at room temperature for 10−30 min. Luciferin reagent was mixed with reconstitution buffer solution. The resuspended samples were treated with 50 μL of the luciferin reagent/buffer mixture and then split in 96-well cell culture plates. After 10 min of incubation at 25 °C, the luminescence of each well was measured with LMaxΠ^{384} (MDS Analytical Technologies, USA), and images were obtained using LAS-1000 (FUGIFILM, Japan). The measurements of luminescence were performed in more than triplicate for accuracy.

Statistical Analysis. Results were analyzed by one-way analysis of variance (ANOVA) and Student's *t*-test using SPSS software. Differences were considered significant for p values of <0.05.

Conflict of Interest: The authors declare no competing financial interest.

Acknowledgment. We thank Soo Cheol Lee for his excellent support to do IPA analysis, and Ms. Geetika Phukan for secretarial assistance in the preparation of the manuscript. This work was supported by the Basic Science Research Program through the National Research Foundation of Korea (NRF) funded by the Ministry of Education, Science, and Technology (2010-0023846 and 2011-0009995), the Priority Research Centers Program through the National Research Foundation of Korea (NRF) funded by the Ministry of Education, Science and Technology (2010-0028294), and 'National Platform Technology Project' supported by Ministry of Knowledge Economy, Republic of Korea.

Supporting Information Available: Table S1: gene list of significantly changed in glutamic acid metabolism. Table S2: gene profiles for RT-PCR confirmation. Table S3: composition percentage of 12 organic acids found in treated 293 cells with MNPs@SiO_2(RITC). Table S4: sequences of gene-specific primer pairs used for RT-PCR. Table S5: sequences of gene-specific primer pairs used for real-time PCR. Figure S1: MTS assay of MNPs@SiO_2(RITC)-treated HEK 293 cells. Figure S2: confocal microscopic appearance of MNPs@SiO_2(RITC)-treated HEK 293 cells. Figure S3: evaluation of uptake efficiency in MNPs@SiO_2-(RITC)-treated cells. Figure S4: intracellular ROS generation of HEK 293 cells after treatment with silica and core NPs. Figure S5: Confocal microscopic appearance of intracellular ROS generation of HEK 293 cells after treatment with silica NPs. Figure S6: confocal microscopic appearance of confirmation of mitochondrial depolarization induced by MNPs@SiO_2(RITC). This material is available free of charge *via* the Internet at http://pubs.acs.org.

REFERENCES AND NOTES

1. Tholouli, E.; Sweeney, E.; Barrow, E.; Clay, V.; Hoyland, J. A.; Byers, R. J. Quantum Dots Light up Pathology. *J. Pathol.* **2008**, *216*, 275–285.
2. Stark, W. J. Nanoparticles in Biological Systems. *Angew. Chem., Int. Ed.* **2011**, *50*, 1242–1258.
3. Hussain, S. M.; Javorina, A. K.; Schrand, A. M.; Duhart, H. M.; Ali, S. F.; Schlager, J. J. The Interaction of Manganese Nanoparticles with PC-12 Cells Induces Dopamine Depletion. *Toxicol. Sci.* **2006**, *92*, 456–463.
4. Jun, Y. W.; Seo, J. W.; Cheon, J. Nanoscaling Laws of Magnetic Nanoparticles and Their Applicabilities in Biomedical Sciences. *Acc. Chem. Res.* **2008**, *41*, 179–189.
5. Amemiya, Y.; Tanaka, T.; Yoza, B.; Matsunaga, T. Novel Detection System for Biomolecules Using Nano-Sized Bacterial Magnetic Particles and Magnetic Force Microscopy. *J. Biotechnol.* **2005**, *120*, 308–314.
6. Horak, D.; Babic, M.; Mackova, H.; Benes, M. J. Preparation and Properties of Magnetic Nano- and Microsized Particles for Biological and Environmental Separations. *J. Sep. Sci.* **2007**, *30*, 1751–1772.
7. McCarthy, J. R.; Kelly, K. A.; Sun, E. Y.; Weissleder, R. Targeted Delivery of Multifunctional Magnetic Nanoparticles. *Nanomedicine* **2007**, *2*, 153–167.
8. Scarberry, K. E.; Dickerson, E. B.; McDonald, J. F.; Zhang, Z. J. Magnetic Nanoparticle-Peptide Conjugates for *In Vitro* and *In Vivo* Targeting and Extraction of Cancer Cells. *J. Am. Chem. Soc.* **2008**, *130*, 10258–10262.
9. Kim, J. S.; Yoon, T. J.; Yu, K. N.; Kim, B. G.; Park, S. J.; Kim, H. W.; Lee, K. H.; Park, S. B.; Lee, J. K.; Cho, M. H. Toxicity and Tissue Distribution of Magnetic Nanoparticles in Mice. *Toxicol. Sci.* **2006**, *89*, 338–347.
10. Gupta, A. K.; Gupta, M. Cytotoxicity Suppression and Cellular Uptake Enhancement of Surface Modified Magnetic Nanoparticles. *Biomaterials* **2005**, *26*, 1565–1573.
11. Morgan, K. Development of a Preliminary Framework for Informing the Risk Analysis and Risk Management of Nanoparticles. *Risk Anal.* **2005**, *25*, 1621–1635.
12. Park, K. S.; Tae, J.; Choi, B.; Kim, Y. S.; Moon, C.; Kim, S. H.; Lee, H. S.; Kim, J.; Park, J.; Lee, J. H.; *et al.* Characterization, *In Vitro* Cytotoxicity Assessment, and *In Vivo* Visualization of Multimodal, RITC-Labeled, Silica-Coated Magnetic Nanoparticles for Labeling Human Cord Blood-Derived Mesenchymal Stem Cells. *Nanomedicine: Nanotechnol., Biol., Med.* **2010**, *6*, 263–276.
13. Cavallero, A.; Marte, A.; Fedele, E. L-Aspartate as an Amino Acid Neurotransmitter: Mechanisms of the Depolarization-Induced Release from Cerebrocortical Synaptosomes. *J. Neurochem.* **2009**, *110*, 924–934.
14. Mathers, D. A.; McCarthy, S. M.; Cooke, J. E.; Ghavanini, A. A.; Puil, E. Effects of the β-Amino Acid Antagonist TAG on Thalamocortical Inhibition. *Neuropharmacology* **2009**, *56*, 1097–1105.
15. Bechet, E.; Guiral, S.; Torres, S.; Mijakovic, I.; Cozzone, A. J.; Grangeasse, C. Tyrosine-Kinases in Bacteria: From a Matter of Controversy to the Status of Key Regulatory Enzymes. *Amino Acids* **2009**, *37*, 499–507.
16. Chuang, D. T.; Chuang, J. L.; Wynn, R. M. Lessons from Genetic Disorders of Branched-Chain Amino Acid Metabolism. *J. Nutr.* **2006**, *136*, 243S–249S.
17. Kimball, S. R.; Jefferson, L. S. Signaling Pathways and Molecular Mechanisms through which Branched-Chain Amino Acids Mediate Translational Control of Protein Synthesis. *J. Nutr.* **2006**, *136*, 227S–231S.
18. Wang, M.; Bai, J.; Chen, W. N.; Ching, C. B. Metabolomic Profiling of Cellular Responses to Carvedilol Enantiomers in Vascular Smooth Muscle Cells. *PLoS One* **2010**, *5*, e15441–e15448.
19. Wang, L.; Xu, D. X.; Lv, Y. G.; Zhang, H. Purification and Biochemical Characterisation of a Novel Glutamate Decarboxylase from Rice Bran. *J. Sci. Food. Agric.* **2010**, *90*, 1027–1033.
20. Spink, D. C.; Wu, S. J.; Martin, D. L. Multiple Forms of Glutamate Decarboxylase in Porcine Brain. *J. Neurochem.* **1983**, *40*, 1113–1119.
21. Zhang, B.; Yuan, Y.; Jia, Y.; Yu, X.; Xu, Q.; Shen, Y. An Association Study between Polymorphisms in Five Genes in Glutamate and GABA Pathway and Paranoid Schizophrenia. *Eur. Psychiatry* **2005**, *20*, 45–49.
22. Schroeder, M. A.; Atherton, H. J.; Ball, D. R.; Cole, M. A.; Heather, L. C.; Griffin, J. L.; Clarke, K.; Radda, G. K.; Tyler, D. J.

Real-Time Assessment of Krebs Cycle Metabolism Using Hyperpolarized ^{13}C Magnetic Resonance Spectroscopy. *FASEB J.* **2009**, *23*, 2529–2538.
23. Sharma, N.; Okere, I. C.; Brunengraber, D. Z.; McElfresh, T. A.; King, K. L.; Sterk, J. P.; Huang, H.; Chandler, M. P.; Stanley, W. C. Regulation of Pyruvate Dehydrogenase Activity and Citric Acid Cycle Intermediates during High Cardiac Power Generation. *J. Physiol.* **2005**, *562*, 593–603.
24. Kobayashi, K.; Neely, J. R. Mechanism of Pyruvate Dehydrogenase Activation by Increased Cardiac Work. *J. Mol. Cell. Cardiol.* **1983**, *15*, 369–382.
25. Yoon, T. J.; Kim, J. S.; Kim, B. G.; Yu, K. N.; Cho, M. H.; Lee, J. K. Multifunctional Nanoparticles Possessing a "Magnetic Motor Effect" for Drug or Gene Delivery. *Angew. Chem., Int. Ed.* **2005**, *44*, 1068–1071.
26. Limbach, L. K.; Li, Y.; Grass, R. N.; Brunner, T. J.; Hintermann, M. A.; Muller, M.; Gunther, D.; Stark, W. J. Oxide Nanoparticle Uptake in Human Lung Fibroblasts: Effects of Particle Size, Agglomeration, and Diffusion at Low Concentrations. *Environ. Sci. Technol.* **2005**, *39*, 9370–9376.
27. Prabha, S.; Zhou, W. Z.; Panyam, J.; Labhasetwar, V. Size-Dependency of Nanoparticle-Mediated Gene Transfection: Studies with Fractionated Nanoparticles. *Int. J. Pharm.* **2002**, *244*, 105–115.
28. Paik, M. J.; Moon, S. M.; Kim, K. R.; Choi, S.; Ahn, Y. H.; Lee, G. Target Metabolic Profiling Analysis of Free Amino Acids in Plasma as EOC/TBDMS Derivatives by GC-SIM-MS. *Biomed. Chromatogr.* **2008**, *22*, 339–342.
29. Self, J. T.; Spencer, T. E.; Johnson, G. A.; Hu, J.; Bazer, F. W.; Wu, G. Glutamine Synthesis in the Developing Porcine Placenta. *Biol. Reprod.* **2004**, *70*, 1444–1451.
30. Burrin, D. G.; Stoll, B. Metabolic Fate and Function of Dietary Glutamate in the Gut. *Am. J. Clin. Nutr.* **2009**, *90*, 850S–856S.
31. Wu, G. Amino Acids: Metabolism, Functions, and Nutrition. *Amino Acids* **2009**, *37*, 1–17.
32. Lin, W.; Huang, Y. W.; Zhou, X. D.; Ma, Y. *In Vitro* Toxicity of Silica Nanoparticles in Human Lung Cancer Cells. *Toxicol. Appl. Pharmacol.* **2006**, *217*, 252–259.
33. Park, E. J.; Choi, J.; Park, Y. K.; Park, K. Oxidative Stress Induced by Cerium Oxide Nanoparticles in Cultured BEAS-2B Cells. *Toxicology* **2008**, *245*, 90–100.
34. Park, E. J.; Park, K. Oxidative Stress and Pro-Inflammatory Responses Induced by Silica Nanoparticles *in Vivo* and *in Vitro*. *Toxicol. Lett.* **2009**, *184*, 18–25.
35. Park, E. J.; Bae, E.; Yi, J.; Kim, Y.; Choi, K.; Lee, S. H.; Yoon, J.; Lee, B. C.; Park, K. Repeated-Dose Toxicity and Inflammatory Responses in Mice by Oral Administration of Silver Nanoparticles. *Environ. Toxicol. Pharmacol.* **2010**, *30*, 162–168.
36. Bauer, A. T.; Strozyk, E. A.; Gorzelanny, C.; Westerhausen, C.; Desch, A.; Schneider, M. F.; Schneider, S. W. Cytotoxicity of Silica Nanoparticles through Exocytosis of Von Willebrand Factor and Necrotic Cell Death in Primary Human Endothelial Cells. *Biomaterials* **2011**, *32*, 8385–8393.
37. Liu, X.; Sun, J. Endothelial Cells Dysfunction Induced by Silica Nanoparticles through Oxidative stress *via* JNK/P53 and NF-κB Pathways. *Biomaterials* **2010**, *31*, 8198–8209.
38. Geys, J.; De Vos, R.; Nemery, B.; Hoet, P. H. *In Vitro* Translocation of Quantum Dots and Influence of Oxidative Stress. *Am. J. Physiol. Lung Cell. Mol. Physiol.* **2009**, *297*, L903–L911.
39. Clichici, S.; Mocan, T.; Filip, A.; Biris, A.; Simon, S.; Daicoviciu, D.; Decea, N.; Parvu, A.; Moldovan, R.; Muresan, A. Blood Oxidative Stress Generation after Intraperitoneal Administration of Functionalized Single-Walled Carbon Nanotubes in Rats. *Acta Physiol. Hung.* **2011**, *98*, 231–241.
40. Shukla, R. K.; Sharma, V.; Pandey, A. K.; Singh, S.; Sultana, S.; Dhawan, A. ROS-Mediated Genotoxicity Induced by Titanium Dioxide Nanoparticles in Human Epidermal Cells. *Toxicol. in Vitro* **2011**, *25*, 231–241.
41. Jeong, Y. S.; Oh, W. K.; Kim, S.; Jang, J. Cellular Uptake, Cytotoxicity, and ROS Generation with Silica/Conducting Polymer Core/Shell Nanospheres. *Biomaterials* **2011**, *32*, 7217–7225.
42. Ye, Y.; Liu, J.; Xu, J.; Sun, L.; Chen, M.; Lan, M. Nano-SiO_2 Induces Apoptosis *via* Activation of p53 and Bax Mediated by Oxidative Stress in Human Hepatic Cell Line. *Toxicol. in Vitro* **2010**, *24*, 751–758.
43. Choi, J.; Zheng, Q.; Katz, H. E.; Guilarte, T. R. Silica-Based Nanoparticle Uptake and Cellular Response by Primary Microglia. *Environ. Health Perspect.* **2010**, *118*, 589–595.
44. Nel, A.; Xia, T.; Madler, L.; Li, N. Toxic Potential of Materials at the Nanolevel. *Science* **2006**, *311*, 622–627.
45. Beck, G. R., Jr.; Ha, S. W.; Camalier, C. E.; Yamaguchi, M.; Li, Y.; Lee, J. K.; Weitzmann, M. N. Bioactive Silica-Based Nanoparticles Stimulate Bone-Forming Osteoblasts, Suppress Bone-Resorbing Osteoclasts, and Enhance Bone Mineral Density *in Vivo*. *Nanomedicine* **2011**, 10.1016/j.nano.2011.11.003.
46. Baber, O.; Jang, M.; Barber, D.; Powers, K. Amorphous Silica Coatings on Magnetic Nanoparticles Enhance Stability and Reduce Toxicity to *In Vitro* BEAS-2B Cells. *Inhal. Toxicol.* **2011**, *23*, 532–543.
47. Udintsev, N. A.; Ivanov, V. V. Antioxidant Action of Glutamic Acid. *Patol. Fiziol. Eksp. Ter.* **1984**, *4*, 60–62.
48. Zhang, D. W.; Shao, J.; Lin, J.; Zhang, N.; Lu, B. J.; Lin, S. C.; Dong, M. Q.; Han, J. RIP3, an Energy Metabolism Regulator that Switches TNF-Induced Cell Death from Apoptosis to Necrosis. *Science* **2009**, *325*, 332–336.
49. Matthews, G. D.; Gur, N.; Koopman, W. J.; Pines, O.; Vardimon, L. Weak Mitochondrial Targeting Sequence Determines Tissue-Specific Subcellular Localization of Glutamine Synthetase in Liver and Brain Cells. *J. Cell. Sci.* **2010**, *123*, 351–359.
50. Smith, D. D., Jr.; Campbell, J. W. Subcellular Location of Chicken Brain Glutamine Synthetase and Comparison with Chicken Liver Mitochondrial Glutamine Synthetase. *J. Biol. Chem.* **1983**, *258*, 12265–12268.
51. Buddhala, C.; Hsu, C. C.; Wu, J. Y. A Novel Mechanism for GABA Synthesis and Packaging into Synaptic Vesicles. *Neurochem. Int.* **2009**, *55*, 9–12.
52. Rubi, B.; Ishihara, H.; Hegardt, F. G.; Wollheim, C. B.; Maechler, P. GAD65-Mediated Glutamate Decarboxylation Reduces Glucose-Stimulated Insulin Secretion in Pancreatic β Cells. *J. Biol. Chem.* **2001**, *276*, 36391–36396.
53. Yoshida, A.; Rzhetsky, A.; Hsu, L. C.; Chang, C. Human Aldehyde Dehydrogenase Gene Family. *Eur. J. Biochem.* **1998**, *251*, 549–557.
54. Hu, C. A.; Lin, W. W.; Valle, D. Cloning, Characterization, and Expression of cDNAs Encoding Human δ1-Pyrroline-5-Carboxylate Dehydrogenase. *J. Biol. Chem.* **1996**, *271*, 9795–9800.
55. Piao, M. J.; Kang, K. A.; Lee, I. K.; Kim, H. S.; Kim, S.; Choi, J. Y.; Choi, J.; Hyun, J. W. Silver Nanoparticles Induce Oxidative Cell Damage in Human Liver Cells through Inhibition of Reduced Glutathione and Induction of Mitochondria-Involved Apoptosis. *Toxicol. Lett.* **2011**, *201*, 92–100.
56. Schaeublin, N. M.; Braydich-Stolle, L. K.; Schrand, A. M.; Miller, J. M.; Hutchison, J.; Schlager, J. J.; Hussain, S. M. Surface Charge of Gold Nanoparticles Mediates Mechanism of Toxicity. *Nanoscale* **2011**, *3*, 410–420.
57. Di Lisa, F.; Blank, P. S.; Colonna, R.; Gambassi, G.; Silverman, H. S.; Stern, M. D.; Hansford, R. G. Mitochondrial Membrane Potential in Single Living Adult Rat Cardiac Myocytes Exposed to Anoxia or Metabolic Inhibition. *J. Physiol.* **1995**, *486*, 1–13.
58. Hsin, Y. H.; Chen, C. F.; Huang, S.; Shih, T. S.; Lai, P. S.; Chueh, P. J. The Apoptotic Effect of Nanosilver Is Mediated by a ROS- and JNK-Dependent Mechanism Involving the Mitochondrial Pathway in NIH3T3 Cells. *Toxicol. Lett.* **2008**, *179*, 130–139.
59. Pan, Y.; Leifert, A.; Ruau, D.; Neuss, S.; Bornemann, J.; Schmid, G.; Brandau, W.; Simon, U.; Jahnen-Dechent, W. Gold Nanoparticles of Diameter 1.4 nm Trigger Necrosis by Oxidative Stress and Mitochondrial Damage. *Small* **2009**, *5*, 2067–2076.
60. Cory, A. H.; Owen, T. C.; Barltrop, J. A.; Cory, J. G. Use of an Aqueous Soluble Tetrazolium/Formazan Assay for Cell Growth Assays in Culture. *Cancer Commun.* **1991**, *3*, 207–212.

61. Paik, M. J.; Cho, E. Y.; Kim, H.; Kim, K. R.; Choi, S.; Ahn, Y. H.; Lee, G. Simultaneous Clinical Monitoring of Lactic Acid, Pyruvic Acid and Ketone Bodies in Plasma as Methoxime/*tert*-butyldimethylsilyl Derivatives by Gas Chromatography−Mass Spectrometry in Selected Ion Monitoring Mode. *Biomed. Chromatogr.* **2008**, *22*, 450–453.
62. Lu, X.; Tian, Y.; Zhao, Q.; Jin, T.; Xiao, S.; Fan, X. Integrated Metabonomics Analysis of the Size-Response Relationship of Silica Nanoparticles-Induced Toxicity in Mice. *Nanotechnology* **2011**, *22*, 055101–055116.
63. Prijic, S.; Scancar, J.; Romih, R.; Cemazar, M.; Bregar, V. B.; Znidarsic, A.; Sersa, G. Increased Cellular Uptake of Biocompatible Superparamagnetic Iron Oxide Nanoparticles into Malignant Cells by an External Magnetic Field. *J. Membr. Biol.* **2010**, *236*, 167–179.
64. Sohaebuddin, S. K.; Thevenot, P. T.; Baker, D.; Eaton, J. W.; Tang, L. Nanomaterial Cytotoxicity Is Composition, Size, and Cell Type Dependent. *Part. Fibre. Toxicol.* **2010**, *7*, 1–17.
65. Hanley, C.; Thurber, A.; Hanna, C.; Punnoose, A.; Zhang, J.; Wingett, D. G. The Influences of Cell Type and ZnO Nanoparticle Size on Immune Cell Cytotoxicity and Cytokine Induction. *Nanoscale Res. Lett.* **2009**, *4*, 1409–1420.
66. Wang, F.; Gao, F.; Lan, M.; Yuan, H.; Huang, Y.; Liu, J. Oxidative Stress Contributes to Silica Nanoparticle-Induced Cytotoxicity in Human Embryonic Kidney Cells. *Toxicol. in Vitro* **2009**, *23*, 808–815.
67. Florea, A. M.; Splettstoesser, F.; Busselberg, D. Arsenic Trioxide (As_2O_3) Induced Calcium Signals and Cytotoxicity in Two Human Cell Lines: SY-5Y Neuroblastoma and 293 Embryonic Kidney (HEK). *Toxicol. Appl. Pharmacol.* **2007**, *220*, 292–301.
68. Yalcin, A. Quantification of Thioredoxin mRNA Expression in the Rat Hippocampus by Real-Time PCR Following Oxidative Stress. *Acta. Biochim. Pol.* **2004**, *51*, 1059–1065.
69. Paik, M. J.; Kim, K. R. Sequential Ethoxycarbonylation, Methoximation and *tert*-Butyldimethylsilylation for Simultaneous Determination of Amino Acids and Carboxylic Acids by Dual-Column Gas Chromatography. *J. Chromatogr., A* **2004**, *1034*, 13–23.
70. Paik, M. J.; Ahn, Y. H.; Lee, P. H.; Kang, H.; Park, C. B.; Choi, S.; Lee, G. Polyamine Patterns in the Cerebrospinal Fluid of Patients with Parkinson's Disease and Multiple System Atrophy. *Clin. Chim. Acta* **2010**, *411*, 1532–1535.
71. Shimizu, N.; Ishii, S. Electron Microscopic Histochemistry of Acetylcholinesterase of Rat Brain by Karnovsky's Method. *Histochemie* **1966**, *6*, 24–33.